Micromaterials and Interfaces (2024) Volume 2 Issue 2
doi: 10.59429/mi.v2i2.6822

RESEARCH ARTICLE

Corrosion resistance assessment of MgAl nanosurface due to doping noble metals: A sustainable approach towards water treatment

Fatemeh Mollaamin*

Department of Biomedical Engineering, Faculty of Engineering and Architecture, Kastamonu University, Kastamonu, 37150, Turkey

*** Corresponding author:** Fatemeh Mollaamin, fmollaamin@kastamonu.edu.tr

ABSTRACT

The corrosion inhibition efficiency of magnesium–aluminum (MgAl) by embedding the noble metals of Ni, Pd, Pt, Cu, Ag, Au on the surface has been investigated. The importance of the electrical double layer at the interface between a metal and an acid electrolyte together with its interaction with organic and inorganic molecules to produce initially electrostatic adsorption are highlighted. The important step in which molecules enable inhibition are production of a physical barrier where a physical adsorbed barrier of molecules prevent movement near the metal surface or decrease in metal reactivity where chemisorbed inhibitor molecules stick to active area on the metal surface. In the NMR spectroscopy, it has been observed the remarkable peaks around metal elements of Ni, Pd, Pt, Cu, Ag, Au through the doping on the MgAl nanoalloy, however there are some fluctuations in the chemical shielding behaviors of isotropic and anisotropy attributes. Furthermore, all accounted ΔG^{o}_{dop} amounts are very close, which demonstrate the agreement of the measured specifications by all methodologies and the reliability of the computing values.

Keywords: noble metal; MgAl; CAM/LANL2DZ; DFT; electron transfer

1. Introduction

These days, pigments and dyes are a serious problem that threatens marine ecology. Annihilating water pollutants by photoactive 2D nanomaterials have indicated promising comparativeness over accessible photocatalysts[1–3]. The researchers have synthesized cobalt oxide (Co_3O_4) with graphite carbon nitride (g-C_3N_4) to make a Co_3O_4@g-C_3N_4 hybrid through a green mechanochemical one-pot synthetic method for manufacturing effective supercapacitor electrodes and photocatalysts[4].

Many resources are accessible to indicate the application of magnesium (Mg) alloys in different engineering areas. Although Mg alloys have the highest strength-to-weight ratio among structural alloys, their balance of characteristics is still the subject of complicated work. Mg alloys have excellent castability, allowing them to be fabricated as complex shapes via procedures with fast production rates, such as high-pressure die casting. Moreover, Mg alloys have superior mechanical attributes and higher thermal conductivity[5–11]. Moreover, density functional theory (DFT) calculation was applied to study the

ARTICLE INFO
Received: 5 September 2024 | Accepted: 2 November 2024 | Available online: 25 November 2024

CITATION
Mollaamin F. Corrosion resistance assessment of MgAl nanosurface due to doping noble metals: A sustainable approach towards water treatment. *Micromaterials and Interfaces* 2024; 2(2): 6822. doi: 10.59429/ima.v2i2.6822

hydrolysis behavior of degradable Mg and Mg alloys, resulting in a good explanation of water adsorption and the stability of the corrosion surface[12–14].

Adsorption involving charged inhibitor species causes a change in the double layer and the potential at the outer Helmholtz plane, influencing the corrosion rates of both anodic and cathodic reactions. The first three modes are intimately with adsorption and the double layer the last involves interaction of the inhibitor molecules and the intermediate products formed during the partial electrochemical reactions, interaction of the adsorbed intermediates with organic molecules can either inhibit or enhance electrode reaction rate depending on the stability of the inhibitor-intermediate complex formed[15,16].

In this study, a new concept of Mg–Al nanoalloy doped with noble metals of Ni, Pd, Pt, Cu, Ag, Au for increasing the corrosion inhibition of the surface is proposed for water remediation such as typical anions and organics as model pollutants by using CAM-B3LYP/ LANL2DZ theoretical methods. Specifically, MgAl alloy reacts with water to produce Mg^{2+}, Al^{3+}, Ni^{2+}, Cu^{o}, and OH^{-} which further adsorbs organic pollutants and other potential secondary pollutants.

2. Designing materials and approaches

2.1. Noble metals & corrosion resistance

The non-heat manageable alloys have the larger corrosion persistence against common corrosion compared to the heat manageable alloys. Nevertheless, the alloys possessing the Al–Mg_2Si system also display notable persistence to usual corrosion process. The identical manner is seen for the alloys that do not consist of Cu in Al–Zn–Mg. The alloys' persistence to pitting corrosion process enhances largely with enhancement of cleanliness[17]. Mg–Al alloys can be doped with some elements consisting of Ni, Pd, Pt, Cu, Ag, Au (**Figure 1**).

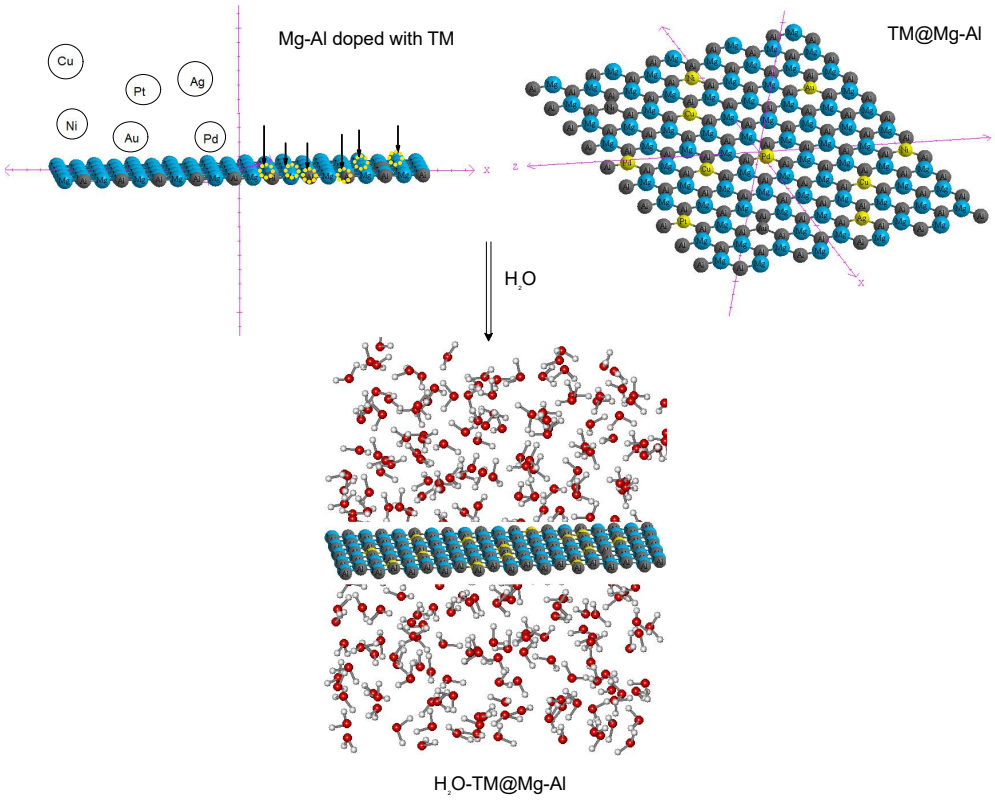

Figure 1. Modeling of noble metals (TM) including Ni, Pd, Pt, Cu, Ag, Au doped on the Mg–Al surface in water

The charge distribution of Mg–Al, Ni@MgAl, Pd@MgAl, Pt@MgAl, Cu@MgAl, Ag@MgAl, and Au@MgAl is calculated due to the Bader charge analysis[18].

2.3. DFT calculations

Our computations have been carried out due to the conceptual density functional theory or DFT[19–21]. Considering the thermal conductivity compared to local density functionals, PBE does not over attach structures, and therefore the interatomic force constants are not too flexible[22]. Hohenberg-Kohn (HK) functions have rigidly made the electronic density permissible as fundamental variable to electronic and structure computations. In other words, development of the applied DFT methodology only became notable after W. Kohn and L. J. Sham released their reputable series of equations which are introduced as Kohn-Sham (KS) equations[23,24]. Considering the electronic density within the KS image directs us to a remarkable reduction of quantum computing. Thus, the KS methodology lightens the route for pursuing systems that cannot be discussed by conventional ab-initio methodologies. Kohn and Sham" introduces the solution which brings up the mono-electronic orbitals to account the kinetic energy in a simple and relatively exact, by founding a residual modification that might be computed apart[23,24]. Therefore, the precise exchange energy functional is described by the Kohn–Sham orbitals in lieu of the density which is cited as the indirect density functional. This research has employed the penetration of the hybrid functional of three-parameter basis set of B3LYP within the conception of DFT upon theoretical computations[25–30].

In this article, the rigid PES using DFT calculations have been accomplished by using Gaussian 16 revision C.01 program package[31]. The input Z-matrix for Mg–Al nanoalloy doped with noble metals of Ni, Pd, Pt, Cu, Ag, Au have been provided with GaussView 6.1[32] due to the rigid system and coordination format of which a blank line has been cited and using LANL2DZ basis set to distinguish chemical shielding, frequencies, thermodynamic properties, electrostatic and electronic potential, natural atomic charges, projected density of state and other quantum properties for this work. In our previous works, it has been accomplished application of DFT calculations through materials modelling[33–52].

3. Results and discussion

3.1. Insight to nuclear quadrupole resonance (NQR)

As the EFG at the citation of the nucleus in N-heterocycles is allocated by the valence electrons twisted in the attachment with close nuclei of TMs–doped Mg–Al nanoalloy, the NQR frequency at which transitions occur is particular for TMs@Mg–Al complex (**Suppl.1**). NQR is a straight frame of the interaction of the quadrupole moment with the EFG which is produced by the electronic structure of its ambiance. Therefore, the NQR transition frequencies are symmetric to the electric quadrupole moment of the nucleus and a measurement of the strength of the local EFG[53–56].

In this research work, the electric potential as the quantity of work energy through carrying over the electric charge from one position to another position in the essence of electric field has been evaluated for Ni@MgAl, Pd@MgAl, Pt@MgAl, Cu@MgAl, Ag@MgAl, Au@MgAl, complexes using CAM-B3LYP/ LANL2DZ level of theory (**Suppl.1**). Furthermore, in **Figure 3** (a–f), it has been sketched the electric potential of nuclear quadrupole resonance for some atoms of aluminum, magnesium, nickel, palladium, platinum, copper, silver, and gold in the doping site on the MgAl alloy surface which has been calculated by CAM–B3LYP/ LANL2DZ.

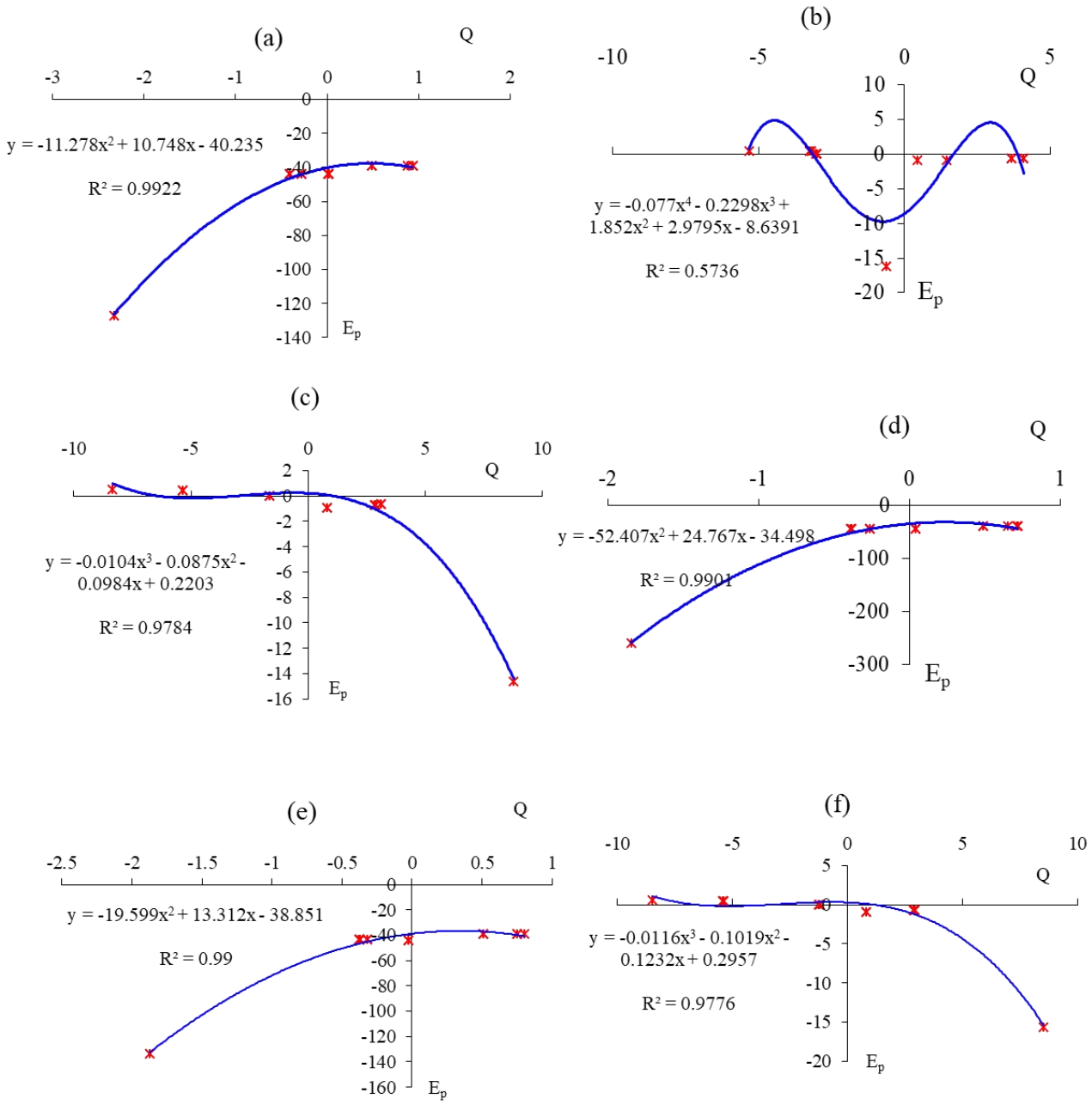

Figure 3. Electric potential (a.u.) versus Bader charge (e) through NQR calculation for the (Ni, Pd, Pt, Cu, Ag, Au)–doped MgAl alloy surface by CAM-B3LYP/LANL2DZ

In **Figure 3** (a–f), it has been described the influence of the replacement of aluminum metal elements in MgAl surface with noble metals of Ni, Pd, Pt, Cu, Ag, Au. However, Figure 3b has indicated a sharp minimum in the value of electric potential (E_p) around –16.2215 a.u. for doping of Pd on the MgAl nanoalloy surface (Pd@MgAl) which can affirm more affinity for electron accepting encountering electron donating compounds.

3.2. Analysis of NMR

From the DFT calculations, it has been attained the chemical shielding (CS) tensors in the principal axes system to estimate the isotropic chemical-shielding (CSI) and anisotropic chemical-shielding (CSA)[57]. The NMR data of isotropic (σ_{iso}), anisotropic shielding tensor (σ_{aniso}) and Bader charge (Q/e) of noble metals

doping of MgAl consisting of Ni@MgAl, Pd@MgAl, Pt@MgAl, Cu@MgAl, Ag@MgAl, Au@MgAl have been computed by Gaussian 16 revision C.01 program package[31] and been shown in **Suppl.2**. Furthermore, **Figure 4** has exhibited the same tendency of shielding for magnesium and aluminum however a considerable deviation from noble metals of nickel (Figure4a), palladium (Figure4b), platinum (Figure4c), copper (Figure4d), silver (Figure4),and gold(Figure4f).

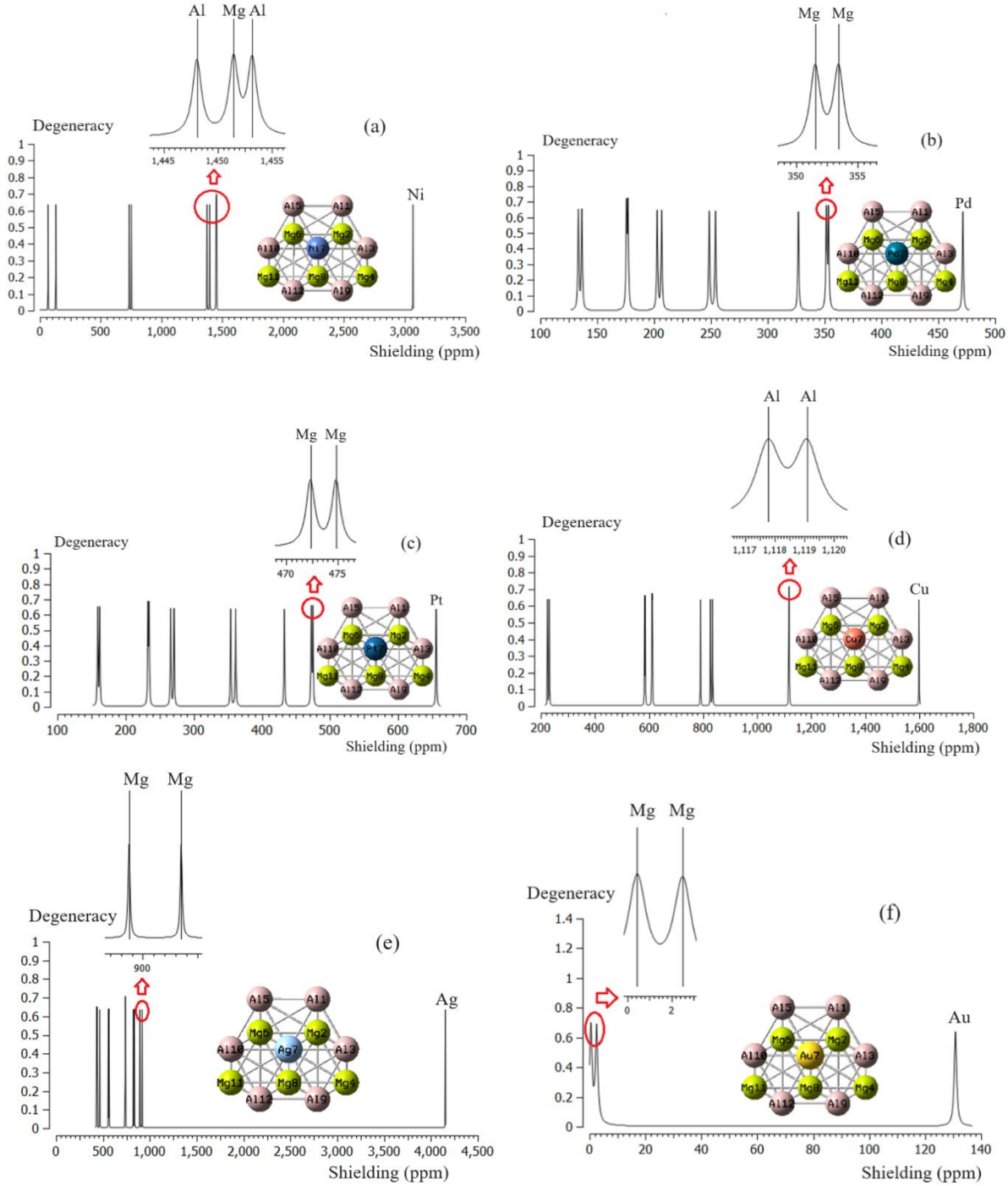

Figure 4. The NMR spectrums for noble metals of Ni, Pd, Pt, Cu, Ag, Au doped on the MgAl nanoalloy surface towards forming complexes of **a)** Ni@MgAl, **b)** Pd@MgAl, **c)** Pt@MgAl, **d)** Cu@MgAl, **e)** Ag@MgAl and **f)** Au@MgAl using CAM-B3LYP/LANL2DZ

In **Figure 4** (a-f), noble metal atoms of Ni, Pd, Pt, Cu, Ag, Au in the complexes of Ni@MgAl (Figure4a), Pd@MgAl (Figure4b), Pt@MgAl (Figure4c), Cu@MgAl (Figure4d), Ag@MgAl (Figure4e), and

Au@MgAl (Figure4e) denote the fluctuation in the chemical shielding. In fact, **Figure 4** (a-f) indicates that the gap chemical shielding between magnesium/aluminum in MgAl nanoalloy surface and noble metals.

3.3. IR analysis

The IR calculations have been accomplished for doping of metal elements of Ni, Pd, Pt, Cu, Ag, Au on the MgAl nanoalloy surface. Therefore, it has been simulated the several clusters containing

Ni@MgAl (Figure5a), Pd@MgAl (Figure5b), Pt@MgAl (Figure5c), Cu@MgAl (Figure5d), Ag@MgAl (Figure5e), and Au@MgAl (Figure5e).

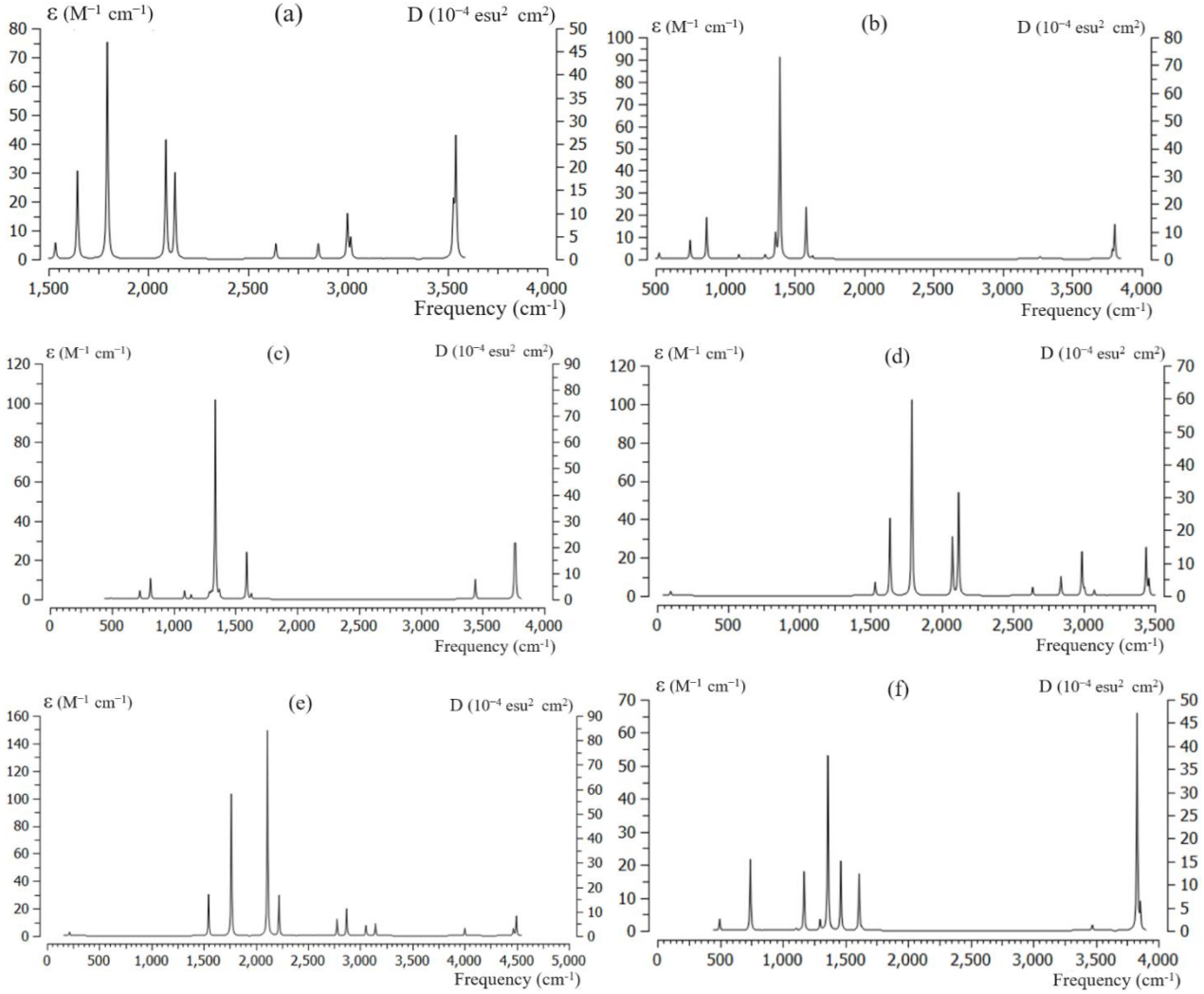

Figure 5. The Frequency (cm^{-1}) changes through the IR spectrums for **a)** Ni@MgAl, **b)** Pd@MgAl, **c)** Pt@MgAl, **d)** Cu@MgAl, **e)** Ag@MgAl, and **f)** Au@MgAl complexes

The spectrum of Figure4 (a) is seen in the frequency range between 1500– 3500 cm^{-1} for Ni@MgAl around 1794.16 cm^{-1}. Figure4 (b) exhibits the frequency range between 1000– 3500 cm^{-1} for Pd@MgAl around 1393.84 cm^{-1}. Figure4 (c) shows the frequency between 1000–4000 cm^{-1} for Pt@MgAl around 1337.17 cm^{-1}. Figure4 (d) demonstrates the frequency between 1500–3500 cm^{-1} for Cu@MgAl around 1791.09 cm^{-1}. Moreover, it is seen the frequency between 1500-4500 for Ag@MgAl around 2110.85 cm^{-1} (Figure4e). Besides, Figure (4f) illustrates the frequency between 1500-4500 for Au@MgAl around 2110.85 cm^{-1}. **Table 1** through the thermodynamic specifications concluded that doped MgAl nanoalloy with noble

metals including Ni, Pd, Pt, Cu, Ag, Au might be more efficient for adsorbing water pollutant due to an adsorption approach.

Table 1. The thermodynamic characters of (Ni,Pd,Pt,Cu,Ag,Au)@MgAl nanosurface using CAM-B3LYP/LANL2DZ calculation.

Compound	$\Delta E^o \times 10^{-4}$ (kcal/mol)	$\Delta H^o \times 10^{-4}$ (kcal/mol)	$\Delta G^o \times 10^{-4}$ (kcal/mol)	S^o (cal/K.mol)	Dipole moment (Debye)
Ni@MgAl	-244.8328	-244.8328	-244.8350	74.120	0.0800
Pd@MgAl	-453.9386	-453.9386	-453.9410	75.724	0.2688
Pt@MgAl	-627.3778	-67.3777	-627.3800	76.488	0.3491
Cu@MgAl	-253.0143	-253.0142	-253.0166	79.123	0.0682
Ag@MgAl	-474.1482	-474.1482	-474.1505	77.910	0.1394
Au@MgAl	-642.3836	-642.3836	-642.3971	77.810	0.4853

The thermodynamic data in **Figure 6** could detect the maximum efficiency of corrosion resistance for doping of MgAl nanoalloy with Ni, Pd, Pt, Cu, Ag, Au through ΔH^o_{dop} which depends on the covalent bond between noble metals and MgAl.

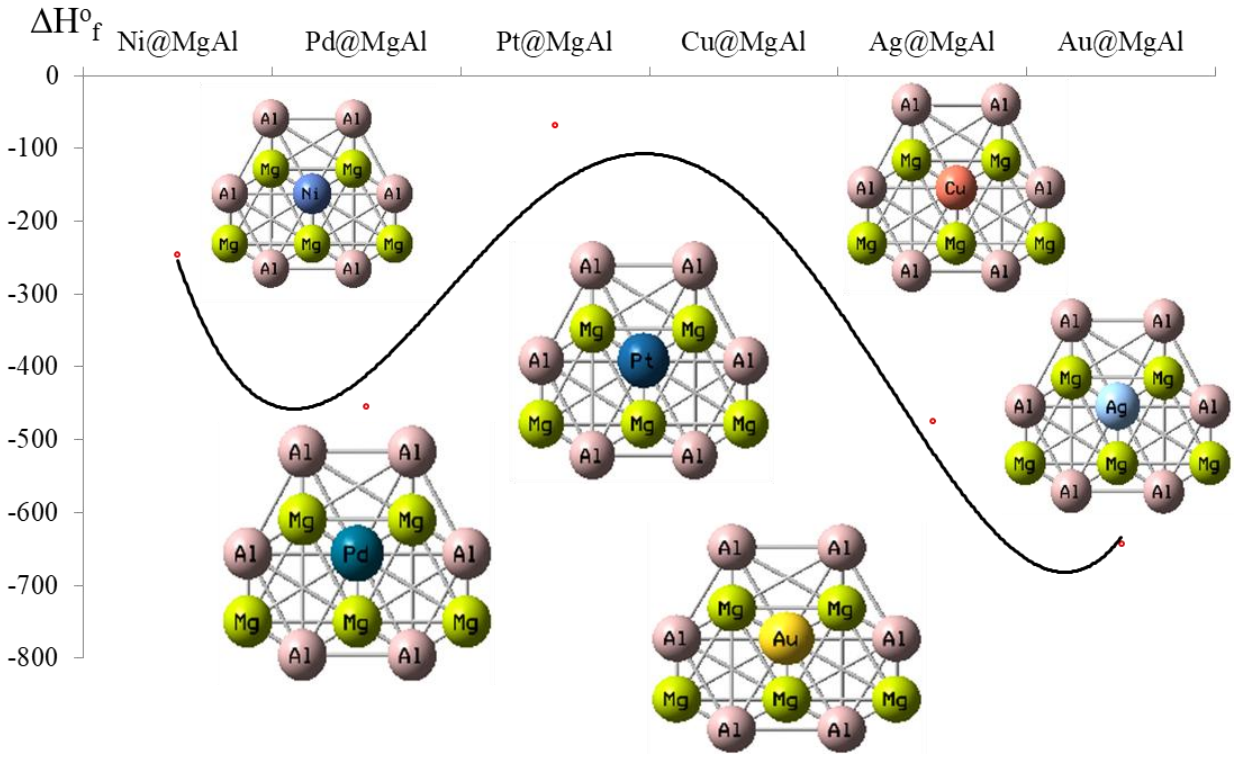

Figure 6. Heat of formation (ΔH^o_{f}) for doping of MgAl with noble metals (X= Ni, Pd, Pt, Cu, Ag, Au) nanoalloy surfaces

The doping process of noble metal on the MgAl nanoalloy surface is affirmed by the ΔH^o_{dop} quantities: $\Delta H^o_{\text{dop}} = \Delta H^o_{\text{X@MgAl}} - \left(\Delta H^o_{\text{X-doped}} + \Delta H^o_{\text{MgAl}}\right)$; $\text{X} = \text{Ni, Pd, Pt, Cu, Ag, Au.}$

4. Conclusion

The efficiency of corrosion inhibition for TM@MgAl has been investigated through the electromagnetic and thermoelectric traits extracts from NMR, NQR, and IR analysis which have been accomplished on Ni@MgAl, Pd@MgAl, Pt@MgAl, Cu@MgAl, Ag@MgAl, Au@MgAl complexes. Examining for corrosion in

the existence of water is also carried out to determine how the presence of water affects the process. In some cases, a chemical bond is formed involving charge transfer or charge sharing between the metal surface and inhibitor molecules forming a coordinate bond through lone-pair electrons on heteroatoms or π electrons on inhibitors with multiple and aromatic bonds.

Acknowledgments

This work was upheld by the investigation in different development destinations for prescient analysis.

Conflict of interest

The creators announce there are no clashes of interest.

References

1. Iqra Rabani, Muhammad Shoaib Tahir, Won-Il Lee, Hai Bang Truong, Ghulam Dastgeer, Young-Soo Seo, Palladium nanoparticle formation on boron nitride nanotubes and their photocatalytic performance with visible light. Journal of Cleaner Production. 420, 138324, 2023. https://doi.org/10.1016/j.jclepro.2023.138324
2. Ramasubba Reddy Palem, Chinna Bathula, Ganesh Shimoga, Soo-Hong Lee, Ayman A. Ghfar, Sankar Sekar, Hyun-Seok Kim, Young-Soo Seo, Iqra Rabani, Fabrication of Ru loaded MgB2 with guar gum hybrid for photocatalytic degradation of crystal violet. International Journal of Biological Macromolecules. 253(3), 126948, 2023. https://doi.org/10.1016/j.ijbiomac.2023.126948
3. Iqra Rabani, Muhammad Shoaib Tahir, Fatima Afzal, Hai Bang Truong, Minsung Kim, Young-Soo Seo, High-efficient mineralization performance of photocatalysis activity towards organic pollutants over ruthenium nanoparticles stabilized by metal organic framework. Journal of Environmental Chemical Engineering. 11(1), 109235, 2023. https://doi.org/10.1016/j.jece.2022.109235
4. Iqra Rabani, Rabia Zafar, K. Subalakshmi, Hyun-Seok Kim, Chinna Bathula, Young-Soo Seo, A facile mechanochemical preparation of Co3O4@g-C3N4 for application in supercapacitors and degradation of pollutants in water. Journal of Hazardous Materials. 407, 124360, 2021. https://doi.org/10.1016/j.jhazmat.2020.124360
5. Wan, Y., Tang, B., Gao, Y., Tang, L., Sha, G., Zhang, B., Liang, N., Liu, C., Jiang, S., Chen, Z.; et al. Bulk nanocrystalline high-strength magnesium alloys prepared via rotary swaging, Acta Mater, 2020, 200, 274–286. https://doi.org/10.1016/j.actamat.2020.09.024.
6. Xin, T., Zhao, Y., Mahjoub, R., Jiang, J., Yadav, A., Nomoto, K., Niu, R., Tang, S., Ji, F., Quadir, Z., et al. Ultrahigh specific strength in a magnesium alloy strengthened by spinodal decomposition, Sci. Adv, 2021, 23, 7. https://doi.org/10.1126/sciadv.abf3039.
7. Javaid, A., Czerwinski, F., Progress in twin roll casting of magnesium alloys: A review, J. Magnes. Alloy, 2021, 9, 362–391. https://doi.org/10.1016/j.jma.2020.10.003.
8. Weiler, J.P., Exploring the concept of castability in magnesium die-casting alloys, J. Magnes. Alloy, 2021, 9, 102–111. https://doi.org/10.1016/j.jma.2020.05.008.
9. Luo, Y., Deng, Y., Guan, L., Ye, L., Guo, X. The microstructure and corrosion resistance of as-extruded Mg-6Gd-2Y-(0–1.5) Nd-0.2Zr alloys, Mater. Des, 2020, 186, 108289. https://doi.org/10.1016/j.matdes.2019.108289.
10. Vanoni, F., Milani, G., Agostoni, C., Treglia, G., Faré, P., Camozzi, P., Lava, S., Bianchetti, M., Janett, S., Magnesium metabolism in chronic alcohol-use disorder: Meta-analysis and systematic review, Nutrients, 2021, 13, 1959. https://doi.org/10.3390/nu13061959.
11. Basri, S., Zulkifli, M.E., Hazri, N.S., Kamarudin, S.K., Quantum Behaviour of Mg and Mg-Al-Zn Microstructure, Crystals, 2023, 13, 501. https://doi.org/10.3390/cryst13030501.

12. Pearton, S.J., Kang, B.S., Kim, S.K., Ren, F.X., Gila, B., Abernathy, C.R., Lin, J., Chu, G., GaN-based diodes and transistors for chemical, gas, biological and pressure sensing, J. Phys. Condens. Matter, 2004, 16, R961–R994. https://doi.org/10.1088/0953-8984/16/29/R02.
13. Mollaamin, F. Monajjemi, M. Application of DFT and TD-DFT on Langmuir Adsorption of Nitrogen and Sulfur Heterocycle Dopants on an Aluminum Surface Decorated with Magnesium and Silicon. Computation. 2023, 11, 108. https://doi.org/10.3390/computation11060108.
14. Mollaamin, F., Monajjemi, M. In Silico-DFT Investigation of Nanocluster Alloys of Al-(Mg, Ge, Sn) Coated by Nitrogen Heterocyclic Carbenes as Corrosion Inhibitors. *J Clust Sci* **34**, 2901–2918 (2023). https://doi.org/10.1007/s10876-023-02436-5
15. Mollaamin, F., Monajjemi, M. Coating of Al–X (X = Mg, Ga, Si) Alloys Nanosurface with Organic Corrosion Inhibitors Using TD-DFT Approach: Intra-Atomic and Interatomic Investigation through Langmuir Adsorption Study. *Russ. J. Phys. Chem. A* 97, 2241–2257 (2023). https://doi.org/10.1134/S0036024423100096
16. Mollaamin, F., Monajjemi, M. Electric and Magnetic Evaluation of Aluminum–Magnesium Nanoalloy Decorated with Germanium Through Heterocyclic Carbenes Adsorption: A Density Functional Theory Study. *Russ. J. Phys. Chem. B* **17**, 658–672 (2023). https://doi.org/10.1134/S1990793123030223
17. Mollaamin, F., Monajjemi, M. Corrosion Inhibiting by Some Organic Heterocyclic Inhibitors Through Langmuir Adsorption Mechanism on the Al-*X* (*X* = Mg/Ga/Si) Alloy Surface: A Study of Quantum Three-Layer Method of CAM-DFT/ONIOM. *J Bio Tribo Corros* **9**, 33 (2023). https://doi.org/10.1007/s40735-023-00751-y
18. Li, S., Dong, H., Wang, X., Liu, Z., Quenching Sensitivity of Al-Zn-Mg Alloy after Non-Isothermal Heat Treatment, Materials, 2019, 12, 1595. https://doi.org/10.3390/ma12101595.
19. Henkelman,G., Arnaldsson,A., Jónsson,H., A fast and robust algorithm for Bader decomposition of charge density, Computational Materials Science, 2006, 36(3), 354-360. https://doi.org/10.1016/j.commatsci.2005.04.010.
20. Blöchl, P.E., Projector augmented-wave method, Phys. Rev. B, 1994, 50, 17953–17979. https://doi.org/10.1103/PhysRevB.50.17953.
21. Perdew, J.P., Burke, K., Ernzerhof, M., Generalized gradient approximation made simple. Phys. Rev. Lett. 1996, 77, 3865. https://doi.org/10.1103/PhysRevLett.77.3865.
22. Ziesche, P., Kurth, S., Perdew, J.P., Density functionals from LDA to GGA, Comput. Mater. Sci, 1998, 11, 122–127. https://doi.org/10.1016/S0927-0256(97)00206-1.
23. Arrigoni, M., Madsen, G.K.H., Comparing the performance of LDA and GGA functionals in predicting the T lattice thermal conductivity of III-V semiconductor materials in the zincblende structure: The cases of AlAs and Bas, Comput. Mater. Sci, 2019, 156, 354–360. https://doi.org/10.1016/j.commatsci.2018.10.005.
24. Hohenberg, P., Kohn, W., Inhomogeneous Electron Gas. Phys. Rev. B, 1964, 136, B864-B871. https://doi.org/10.1103/PhysRev.136.B864.
25. Kohn, W., Sham, L. J., Self-Consistent Equations Including Exchange and Correlation Effects.Phys. Rev., 1965, 140, A1133- A1138. https://doi.org/10.1103/PhysRev.140.A1133.
26. Becke, A.D.,Density-functional thermochemistry. III. The role of exact exchange, J Chem Phys, 1993, 98, 5648–5652. https://doi.org/10.1063/1.464913.
27. Lee, C., Yang, W., Parr, R.G., Development of the Colle–Salvetti correlation-energy formula into a functional of the electron density, Phys Rev B, 1988, 37, 785–789. https://doi.org/10.1103/PhysRevB.37.785.
28. Mollaamina,F., Mohammadi,S., Khalaj, Z., Monajjemi,M., Computational Modelling of Boron Nitride Nanosheet for Detecting and Trapping of Water Contaminant, Russ. J. Phys. Chem. B, 2024, 18 (1), 67–82. https://doi.org/10.1134/S1990793124010330

29. Stephens, P.J., Devlin, F.J., Chabalowski, C.F., Frisch, M.J., Ab Initio Calculation of Vibrational Absorption and Circular Dichroism Spectra Using Density Functional Force Fields, J. Phys. Chem, 1994, 98 (45), 11623–11627. https://doi.org/10.1021/j100096a001.
30. Cramer, C.J., Essentials of Computational Chemistry: Theories and Models, 2nd Edition Wiley. Wiley.com. Retrieved 2021-06-24, 2004.
31. Vosko, S.H., Wilk, L., Nusair, M., Accurate spin-dependent electron liquid correlation energies for local spin density calculations: a critical analysis, Can. J. Phys, 1980, 58 (8), 1200–1211. https://doi.org/10.1139/p80-159.
32. Frisch, M. J., Trucks, G. W., Schlegel, H. B., Scuseria, G. E., Robb, M. A., et al., Gaussian 16, Revision C.01, Gaussian, Inc., Wallingford CT, 2016.
33. Dennington, R., Keith, T.A., Millam, J.M., GaussView. Version 6. Shawnee Mission (KS): Semichem Inc., 2016.
34. Monajjemi, M., Mahdavian, L., Mollaamin, F., Khaleghian, M., Interaction of Na, Mg, Al, Si with carbon nanotube (CNT): NMR and IR study, Russ. J. Inorg. Chem,2009, 54, 1465–1473. https://doi.org/10.1134/S0036023609090216.
35. Bakhshi, K., Mollaamin,F., Monajjemi, M., Exchange and Correlation Effect of Hydrogen Chemisorption on Nano V(100) Surface: A DFT Study by Generalized Gradient Approximation (GGA), J. Comput. Theor. Nanosci, 2011, 8, 763–768. https://doi.org/10.1166/JCTN.2011.1750.
36. Mollaamin, F. Competitive intracellular hydrogen-nanocarrier among aluminum, carbon, or silicon implantation: A novel technology of eco-friendly energy storage using research density functional theory. Russ J Phys Chem B. 2024, 18, 805-820. https://doi.org/10.1134/S1990793124700131.
37. Mollaamin, F., Monajjemi, M., Harmonic Linear Combination and Normal Mode Analysis of Semiconductor Nanotubes Vibrations, J. Comput. Theor. Nanosci, 2015, 12, 1030-1039. https://doi.org/10.1166/jctn.2015.3846.
38. Zadeh, M.A.A., Lari, H., Kharghanian, L., Balali, E., Khadivi, R., Yahyaei, H.,Mollaamin, F., Monajjemi, M., Density functional theory study and anti-cancer properties of shyshaq plant: In view point of nano biotechnology, J. Comput. Theor. Nanosci 2015, 12, 4358–4367, https://doi.org/10.1166/jctn.2015.4366.
39. Monajjemi, M., Baie, M.T., Mollaamin, F., Interaction between threonine and cadmium cation in [Cd(Thr)] (n = 1-3) complexes: Density functional calculations, Russian Chemical Bulletin, 2010, 59, 886-889. https://doi.org/10.1007/s11172-010-0181-5.
40. Monajjemi, M., Khaleghian, M., Tadayonpour, N., Mollaamin, F., The effect of different solvents and temperatures on stability of single-walled carbon nanotube: A QM/MD study, Int. J. Nanosci, 2010, 09, 517-529, https://doi.org/10.1142/S0219581X10007071.
41. Tahan, A., Mollaamin, F., Monajjemi, M., Thermochemistry and NBO analysis of peptide bond: Investigation of basis sets and binding energy, Russian Journal of Physical Chemistry A, 2009, 83, 587-597, https://doi.org/10.1134/S003602440904013X.
42. Mollaamin, F., Monajjemi, M., Trapping of toxic heavy metals from water by GN–nanocage: Application of nanomaterials for contaminant removal technique, J. Mol. Struct, 2024, 1300, 137214. https://doi.org/10.1016/j.molstruc.2023.137214.
43. Mollaamin, F., Ilkhani, A., Sakhaei, N., Bonsakhteh, B., Faridchehr, A., Tohidi, S., Monajjemi, M.,Thermodynamic and solvent effect on dynamic structures of nano bilayer-cell membrane: Hydrogen bonding study, Journal of Computational and Theoretical Nanoscience, 2015, 12, 3148-3154. https://doi.org/10.1166/jctn.2015.4092.
44. Mollaamin,F., Majid Monajjemi,M., Molecular simulation of (Al–Ga) surface garnished with chromium metal for organic material detecting: A DFT study. Functional Materials Letters, 2023, 16(07), 2340028. https://doi.org/10.1142/S1793604723400283.

45. Khalili Hadad, B., Mollaamin, F., Monajjemi, M. Biophysical chemistry of macrocycles for drug delivery: A theoretical study. Russian Chemical Bulletin, 2011,60, 238-241, https://doi.org/10.1007/s11172-011-0039-5.
46. Mollaamin, F., Features of Parametric Point Nuclear Magnetic Resonance of Metals Implantation on Boron Nitride Nanotube by Density Functional Theory/Electron Paramagnetic Resonance. Journal of Computational and Theoretical Nanoscience, 11(11), 2014, 2393–2398. https://doi.org/10.1166/jctn.2014.3653.
47. Mollaamin, F., Monajjemi, M., In Situ Ti-Embedded SiC as Chemiresistive Nanosensor for Safety Monitoring of CO, CO2, NO, NO2: Molecular Modelling by Conceptual Density Functional Theory, Russ. J. Phys. Chem. B, 2024, 18 (1), 49–66. https://doi.org/10.1134/S1990793124010159.
48. Sarasia, E.M., Afsharnezhad, S., Honarparvar, B., Mollaamin, F.,Monajjemi, M., Theoretical study of solvent effect on NMR shielding tensors of luciferin derivatives, Phys Chem Liquids, 2011, 49, 561–571, https://doi.org/10.1080/00319101003698992.
49. Shahriari, S., Mollaamin, F., Monajjemi, M., Increasing the Performance of {[(1-x-y) $LiCo_{0.3}Cu_{0.7}$] (Al and Mg doped)] O_2}, xLi_2MnO_3, $yLiCoO_2$ Composites as Cathode Material in Lithium-Ion Battery: Synthesis and Characterization. Micromachines 2023, 14, 241. https://doi.org/10.3390/mi14020241.
50. Monajjemi, M., Mollaamin,F., Shojaei, S., An overview on Coronaviruses family from past to Covid-19: Introduce some inhibitors as antiviruses from Gillan's plants, Biointerface Res. Appl. Chem, 2020, 10, 5575. https://doi.org/10.33263/BRIAC103.575585.
51. Mollaamin, F., Monajjemi, M., Tailoring and functionalizing the graphitic-like GaN and GaP nanostructures as selective sensors for NO, NO_2, and NH_3 adsorbing: a DFT study, J Mol Model, 2023, 29, 170. https://doi.org/10.1007/s00894-023-05567-8.
52. Mollaamin, F., Monajjemi, M., Transition metal (X = Mn, Fe, Co, Ni, Cu, Zn)-doped graphene as gas sensor for CO_2 and NO_2 detection: a molecular modeling framework by DFT perspective, J Mol Model, 2023, 29, 119 (2023). https://doi.org/10.1007/s00894-023-05526-3.
53. Mollaamin, F., Monajjemi, M., Graphene-based resistant sensor decorated with Mn, Co, Cu for nitric oxide detection: Langmuir adsorption & DFT method, Sensor Review, 2023, 43, 266–279. https://doi.org/10.1108/SR-03-2023-0040.
54. Trontelj, Z.; Pirnat, J.; Jazbinšek, V.; Lužnik, J.; Srčič, S.; Lavrič, Z.; Beguš, S.; Apih, T.; Žagar, V.; Seliger, J. Nuclear Quadrupole Resonance (NQR)—A Useful Spectroscopic Tool in Pharmacy for the Study of Polymorphism. Crystals 2020, 10, 450. https://doi.org/10.3390/cryst10060450.
55. Sciotto, R.; Ruiz Alvarado, I.A.; Schmidt, W.G. Substrate Doping and Defect Influence on P-Rich InP(001):H Surface Properties. Surfaces 2024, 7, 79-87. https://doi.org/10.3390/surfaces7010006
56. Luo,J., Wang,C., Wang,Z., Guo,Q., Yang,J., Rui Zhou, R., Matano,K., Oguchi,T., Ren, Z., NMR and NQR studies on transition-metal arsenide superconductors LaRu2As2, KCa2Fe4As4F2, and A2Cr3As3*, Chinese Physm, 2020, B 29, 067402. https://doi.org/10.1088/1674-1056/ab892d.
57. Young, Hugh A.; Freedman, Roger D. (2012). Sears and Zemansky's University Physics with Modern Physics (13^{th} ed.). Boston: Addison-Wesley. p. 754.
58. Sohail, U., Ullah, F., Binti Zainal Arfan, N.H., Abdul Hamid, M.H.S., Mahmood, T., Sheikh, N.S., Ayub, K., Transition Metal Sensing with Nitrogenated Holey Graphene: A First-Principles Investigation, Molecules, 2023, 28, 4060. https://doi.org/10.3390/molecules28104060.

Suppl.1. The electric potential (au) and Bader charge (e) through NQR calculation for (Ni/Pd/Pt,Cu/Ag/Au)@Mg–Al nanosurface using CAM-B3LYP/LANL2DZ calculation.

Ni@ Mg–Al			**Pd Mg–Al**			**Pt Mg–Al**		
Atom	**Q**	**E_p**	**Atom**	**Q**	**E_p**	**Atom**	**Q**	**E_p**
Al1	0.01	–43.72	Al1	0.46	–0.95	Al1	0.82	–0.94
Mg2	0.93	–38.78	Mg2	–3.25	0.38	Mg2	–5.36	0.47
Al3	–0.41	–43.63	Al3	4.09	–0.67	Al3	3.11	–0.65
Mg4	0.48	–39.00	Mg4	–3.00	–0.00	Mg4	–1.64	0.00
Al5	0.01	–43.72	Al5	1.45	–0.95	Al5	0.82	–0.94
Mg6	0.93	–38.78	Mg6	–3.18	0.38	Mg6	–5.34	0.46
Ni7	–2.33	–127.02	Pd7	–0.61	–16.22	Pt7	8.76	–14.59
Mg8	0.87	–38.77	Mg8	–5.33	0.41	Mg8	–8.33	0.50
Al9	–0.28	–43.57	Al9	3.66	–0.69	Al9	2.85	–0.68
Al10	–0.41	–43.64	Al10	4.06	–0.67	Al10	3.11	–0.66
Mg11	0.48	–39.00	Mg11	–3.02	–0.00	Mg11	–1.66	0.00
Al12	–0.28	–43.57	Al12	3.67	–0.69	Al12	2.86	–0.68
Cu Mg–Al			**Ag Mg–Al**			**Au Mg–Al**		
Atom	**Q**	**E_p**	**Atom**	**Q**	**E_p**	**Atom**	**Q**	**E_p**
Al1	0.04	–43.75	Al1	–0.02	–43.72	Al1	0.81	–0.93
Mg2	0.71	–38.79	Mg2	0.75	–38.74	Mg2	–5.41	0.53
Al3	–0.38	–43.58	Al3	–0.32	–43.63	Al3	2.93	–0.68
Mg4	0.48	–38.97	Mg4	0.51	–39.00	Mg4	–1.23	–0.00
Al5	0.04	–43.75	Al5	–0.03	–43.72	Al5	0.81	–0.93
Mg6	0.71	–38.79	Mg6	0.75	–38.75	Mg6	–5.39	0.52
Cu7	–1.84	–260.55	Ag7	–1.87	–133.42	Au7	8.52	–15.60
Mg8	0.65	–38.74	Mg8	0.80	–38.72	Mg8	–8.47	0.56
Al9	–0.26	–43.62	Al9	–0.37	–43.58	Al9	2.86	–0.66
Al10	–0.38	–43.58	Al10	–0.32	–43.63	Al10	2.93	–0.68
Mg11	0.49	–38.98	Mg11	0.51	–39.00	Mg11	–1.26	–0.00
Al12	–0.26	–43.62	Al12	–0.37	–43.58	Al12	2.87	–0.66
Al1	0.04	–43.75	Al1	–0.02	–43.72	Al1	0.81	–0.93

Suppl.2. Data of NMR shielding tensors for selected atoms of (Ni,Pd,Pt,Cu,Ag,Au)@ MgAl nanosurface using CAM-B3LYP/LANL2DZ calculation.

Ni@MgAl			**Pd@MgAl**			**Pt@MgAl**		
Atom	**σ_{iso}**	**σ_{aniso}**	**Atom**	**σ_{iso}**	**σ_{aniso}**	**Atom**	**σ_{iso}**	**σ_{aniso}**
Al1	129.50	4308.75	Al1	254.00	395.99	Al1	361.47	622.46
Mg2	1396.53	1397.03	Mg2	353.45	686.03	Mg2	474.82	876.99
Al3	1448.07	1185.23	Al3	177.07	349.88	Al3	234.53	427.58
Mg4	733.60	1043.41	Mg4	133.41	231.96	Mg4	159.06	268.63
Al5	65.34	4139.96	Al5	248.51	375.12	Al5	354.22	597.72
Mg6	1373.49	1274.30	Mg6	351.53	686.92	Mg6	472.35	878.02
Ni7	3069.06	15618.11	Pd7	471.59	890.51	Pt7	655.70	1198.03
Mg8	1451.45	1266.72	Mg8	326.90	671.61	Mg8	432.90	865.60
Al9	443.80	3165.94	Al9	202.77	261.00	Al9	266.12	290.82
Al10	1453.17	1192.18	Al10	175.80	349.86	Al10	232.85	427.11
Mg11	751.841	967.03	Mg11	136.49	227.19	Mg11	162.04	263.51
Al12	403.60	2999.65	Al12	206.62	256.15	Al12	271.11	284.60
Cu@MgAl			**Ag@MgAl**			**Au@MgAl**		
Atom	**σ_{iso}**	**σ_{aniso}**	**Atom**	**σ_{iso}**	**σ_{aniso}**	**Atom**	**σ_{iso}**	**σ_{aniso}**
Al1	224.72	1436.10	Al1	436.08	1134.00	Al1	5.73	61.53
Mg2	612.43	128.07	Mg2	739.49	364.12	Mg2	33.32	138.91
Al3	1119.08	321.45	Al3	563.33	632.45	Al3	15.91	73.90
Mg4	827.35	827.35	Mg4	893.63	249.31	Mg4	0.45	47.47
Al5	231.54	1423.72	Al5	464.89	1095.14	Al5	3.06	62.73
Mg6	610.44	126.85	Mg6	738.08	363.50	Mg6	33.24	135.54
Cu7	1599.30	1550.61	Ag7	4153.47	800.70	Au7	130.84	120.29
Mg8	790.99	416.94	Mg8	432.80	480.68	Mg8	26.71	108.86
Al9	586.23	823.97	Al9	834.82	441.50	Al9	4.35	50.65
Al10	1117.77	326.76	Al10	557.53	633.34	Al10	16.56	72.75
Mg11	835.35	544.10	Mg11	917.62	223.14	Mg11	2.50	45.16
Al12	583.76	826.41	Al12	824.07	458.26	Al12	5.05	47.75